The Orbitofrontal Cortex Represents Advantageous Choice in the Iowa Gambling Task

Rujing Zha
University of Science and Technology of China https://orcid.org/0000-0003-0457-096X
Peng Li
University of Science and Technology of China
Ying Li
University of Science and Technology of China
Nan Li
University of Science and Technology of China
Meijun Gao
University of Science and Technology of China https://orcid.org/0000-0002-2584-5718
Yiyang Fan
University of Science and Technology of China
Ruhuiya Aili
University of Science and Technology of China
Ying Liu
Xiaochu Zhang (zxcustc@ustc.edu.cn)
University of Science and Technology of China https://orcid.org/0000-0002-7541-0130
Jun Li
University of Science and Technology of China

Article

Keywords: orbitofrontal cortex, advantageous choice, multivoxel pattern analysis, psycho-physiological interaction, fMRI

Posted Date: May 27th, 2021

DOI: https://doi.org/10.21203/rs.3.rs-523769/v1

The orbitofrontal cortex represents advantageous choice in the Iowa gambling task

Rujing Zha[1#], Peng Li[2#], Ying Li[1], Nan Li[1], Meijun Gao[3], Yiyang Fan[1], Ruhuiya Aili[4], Ying Liu[5], Xiaochu Zhang[1*], Jun Li[6*]

[1]Key Laboratory of Brain Function and Disease, Chinese Academy of Sciences, School of Life Sciences, University of Science & Technology of China, Hefei, Anhui 230027, China

[2]Department of Automation, School of Information Science and Technology, University of Science and Technology of China, Hefei, Anhui 230027, China

[3]Department of Computer Science and Engineering, Michigan State University, East Lansing, MI 48824, USA

[4]School of Chemistry, University of Science & Technology of China, Hefei, Anhui 230027, China

[5]Anhui Medical University, Hefei, Anhui, 230001, China

[6]Department of Automation, University of Science and Technology of China, Hefei 230027, China

[#]Co-first authors.

[*]Address correspondence to Jun Li, Department of Automation, University of Science and Technology of China, Hefei 230027, China. Telephone: +86-551-6360-1999. Email: ljun@ustc.edu.cn (J. Li), and Xiaochu Zhang, School of Life Sciences, University of Science & Technology of China, Hefei, Anhui 230027, China. Telephone: +86-551-6360-7295. Email: zxcustc@ustc.edu.cn (X. Zhang)

Abstract

A good-based model proposes that the orbitofrontal cortex (OFC) represents binary choice outcome, i.e., the chosen good. Previous studies have found that the OFC represents the binary choice outcome in decision-making tasks involving commodity type, cost, risk, and delay. Real-life decisions are often complex and involve uncertainty, rewards, and penalties; however, whether the OFC represents binary choice outcomes in a such decision-making situation, e.g., Iowa gambling task (IGT), remains unclear. Here, we propose that the OFC represents binary choice outcome, i.e., advantageous choice versus disadvantageous choice, in the IGT. We propose two hypotheses: first, the activity pattern in the human OFC represents an advantageous choice; and second, choice induces an OFC-related functional network. Using functional magnetic resonance imaging and advanced machine learning tools, we found that the OFC represented an advantageous choice in the IGT. The OFC representation of advantageous choice was related to decision-making performance. Choice modulated the functional connectivity between the OFC and the superior medial gyrus. In conclusion, the OFC represents an advantageous choice during the IGT. In the framework of a good-based model, the results extend the role of the OFC to complex decision-making when making a binary choice.

Keywords: orbitofrontal cortex, advantageous choice, multivoxel pattern analysis, psycho-physiological interaction, fMRI

Introduction

The identified neurobiological mechanism underlying economic decision-making includes a valuation stage and a choice stage[1-3]. Decision makers evaluate the subjective values and characteristics of available options in the valuation stage. However, encoding subjective value and characteristics is not sufficient for making decisions, and one of the available options still needs to be chosen by decision makers at the choice stage[1-3]. At this stage, a good-based model, a central neurobiological model of economic decision-making, proposes that the orbitofrontal cortex (OFC) represents the binary choice outcome, i.e., the chosen good[4]. A good is defined by a group of determinants characterizing the conditions in which the commodity is offered, which can include commodity type, time delay, cost, risk, and ambiguity[4].

Consistent with a good-based model, previous studies have found that the OFC represents the binary choice outcome in juice-choice tasks[5] and decision-making tasks involving costs[6], risks[7], and delays[8]. For example, different OFC neurons respond when a monkey chooses between different juice types[5]. Some OFC neuronal responses in monkeys encode choosing a high-cost option versus choosing a low-cost option[6]. Some other OFC neurons in monkeys encode choosing a risky option versus choosing a nonrisky option[7]. The OFC activity pattern in the human brain can classify choosing smaller-but-immediate options versus choosing larger-but-delayed options[8]. However, real-life decisions are often complex and involve uncertainty, rewards, and penalties.

The inability to make choices in a complex decision-making situation, e.g., Iowa gambling task (IGT), is a symptom of several brain disorders, including borderline personality disorder[9], attention-

deficit/hyperactivity disorder[9], anorexia nervosa[10], addiction[11], obsessive-compulsive disorder[12], and schizophrenia[13]. In the IGT, reward value is a key decision-making parameter[14]. Whether the OFC represents a binary choice outcome in the IGT, advantageous choice (i.e., choosing an option with a high reward value) versus disadvantageous choice (i.e., choosing an option with a low reward value), remains unclear.

A line of studies has implicated the OFC at the valuation stage, i.e., evaluating available options such as the value[15-18], risk[19,20], ambiguity[21,22], and environmental statistics[23]. For example, Hare et al. and Kable et al. reported that OFC activity was correlated with high values versus low values[24,25]. Both Bartra et al. and Clithero et al. have shown that the OFC is a key brain area related to high subjective values versus low subjective values of different types of rewards using meta-analysis[26,27]. Some studies have also investigated the neural basis of high ambiguity versus low ambiguity in decision-making. For example, Levy et al. showed that OFC activity is correlated with ambiguity level[21]. Hsu et al. also revealed that the OFC showed greater activation in response to the level of ambiguity[22]. Huettel et al. found increased activation in the inferior frontal sulcus, insula, and parietal cortex when ambiguity was present[28]. Bach et al. found that ambiguity is related to parietal cortex activity[29]. Therefore, these studies have implicated the OFC in evaluating risk, ambiguity, and value.

Another line of neurobiological studies investigated advantageous versus disadvantageous choice in the IGT; however, they found that blood oxygenation level-dependent (BOLD) activation using individual voxel-based methods in the OFC was not significantly associated with advantageous choice versus disadvantageous choice[30-40]. For example, Brevers et al. did not find any advantageous choice-related

activation in the OFC in healthy controls or poker gamblers in the IGT[37]. One potential explanation for the finding that the OFC was not implicated in advantageous choice in the IGT in these studies is that ensembles of many voxels, rather than single voxel activation, are responsible for generating economic choices. For example, multiple voxels in the OFC were shown to contain information on the discrimination between choosing a larger-but-delayed option and chossing a smaller-but-immediate option in decision-making involving delays[8]. Therefore, the individual-voxel-based methods used by previous studies might not be suitable. As multivoxel pattern analysis (MVPA) can detect fine-grained spatial patterns across multiple voxels that might discriminate between cognitive processes[41], it may be a potential method to detect advantageous choice in the OFC in the IGT. Therefore, in the present study, we hypothesized that the OFC represented advantageous choice in the IGT.

Methods

Participants. Fifty-five healthy participants were recruited in the study, and one participant was excluded after presenting with significant head motion (>3.0 mm) during functional magnetic resonance imaging (fMRI) scanning. The remaining fifty-four participants included 45 males and nine females [age: mean, 22.7 years; standard deviation (SD), 2.1 years; range, 19 to 27 years; education: mean, 16.3 years; SD, 1.8 years; range, 13 to 19 years]. All participants were free of psychiatric or neurological history and had normal or corrected-to-normal vision. The study was approved by the Human Research Ethics Committee of the University of Science and Technology of China. The methods and procedures used in this study were carried out in accordance with the approved guidelines. Written informed consent was obtained from all participants before the study, consistent with the Declaration of Helsinki guidelines.

Task paradigm. In the present study, we used the Iowa gambling task (IGT)[14] (Fig. 1), a popular decision-making task for indexing real-life complex decision-making. In each trial, the participants selected a card from among four decks of cards. The four decks were labelled A, B, C, and D as presented from left to right. On each card, there were different numbers of gain and possible loss points, and the participant received the net (gain - loss) points for choosing that card. Participants did not know the expected reward and variability in the outcomes for all decks before engaging in the task. In the task, the participants were asked to maximize the points they gained. Specifically, for each selection from deck A or B ("low reward value decks"), participants would gain 100 points, but the losses were organized so that over 10 selections from the decks, the participants would have an overall loss of 250 points. Specifically, deck A provided -150, -200, -250, -300 and -350 (loss) points every ten selections, whereas deck B provided -1250 (loss) points in one out of ten selections. For each selection from deck C or D ("high reward value decks"), the participants would win 50 points, and the losses were organized so that if participants made over 10 selections from these decks, they would obtain an overall profit of 250 points. The two decks differed in the frequency and magnitude of the punishment. Similar to the previous two decks, deck C provided -25, -40, -50, -60 and -75 (loss) points every ten selections, whereas deck D provided -250 (loss) points once every ten selections. Decks A and B had negative reward expectations and were operationally defined as having a low reward value. In contrast, decks C and D had positive reward expectations and were defined as having a high reward value. Therefore,

choosing decks C and D was an advantageous choice, and choosing decks A and B was a disadvantageous choice. Similar to previous studies[42,43], the IGT was extended to 180 trials from the original 100 trials to facilitate rule learning[14]. The IGT consisted of three scan runs, with three blocks for each scan run and 20 trials for each block. The participants who had positive net winnings at the end of the task would obtain extra money (10¥/1000 points). The final net winnings were defined as the total score.

Behavioural analysis—reinforcement learning model. This procedure followed that of a previous study[43]. The reinforcement learning model[44] was adapted to analyse the behavioural data. Reward prediction errors (RPEs) were included in the model, according to the suggestion by Sutton and Barto[45]. An RPE (δ_t) was defined as the difference between the actual reward r_t and the predicted reward $\hat{v}_t$ at trial t. The formula for this definition was as follows:

$$\delta_t = r_t - \hat{v}_t. \quad (1)$$

The RPE was used to update reward prediction in the model using the following formula:

$$\hat{v}_{t+1} = \hat{v}_t + \alpha \cdot \delta_t. \quad (2)$$

where α is the learning rate for the RPE in the update formula[44]. Then, maximum likelihood estimation (MLE) was adopted to estimate the learning rate based on the samples. Here, π_{it} was defined as the probability of choice i at trial t. We transformed the data with an exponential function when we calculated the value of π_{it} using the following formula:

$$\pi_{it} = \frac{e^{\hat{v}_{it}}}{\sum_{j=1}^{n} e^{\hat{v}_{jt}}}. \quad (3)$$

The learning rate was estimated separately by maximizing the likelihood function for each participant:

$$\text{Maximum } \log-\text{likelihood} = \max \sum_{t=1}^{M} \log \pi_{i_t,t} \quad (4)$$

where i_t represents the deck selected at trial t, $i_t \in \{1,\ 2,\ 3,\ 4\}$, and $\pi_{i_t,t}$ represents the probability of selecting deck i_t at trial t.

To test whether the participants' decision-making performance was better than random chance, we performed a random selection simulation 1000 times. We compared the learning rate from the participants' choices with that from the simulation using the t test. We tested group differences using t test if data conformed normality and using Mann-Whitney test if data do not conform normality in the

present study. Cohen's d values were calculated via G*Power 3.1 software[46]. We calculated the total net good decks, which was the number of advantageous choices minus the number of disadvantageous choices in 180 trials.

fMRI data acquisition and preprocessing. Gradient echo-planar imaging data were acquired using a 3.0 T, 8-channel head coil Trio scanner (Siemens Medical Solution, Erlangen, Germany) with a circularly polarized head coil in Hefei. We restrained head motion with foam padding. A T2*-weighted echo-planar imaging sequence (FOV = 240 mm, TE = 30 ms, TR = 2000 ms, flip angle = 85°, matrix = 64 $\times$ 64) with 33 axial slices (no gaps, 3.7 mm thick) covering the whole brain was used to acquire the functional MR images. There were three runs of IGT, each of which contained 210 epochs. Furthermore, high-resolution T1-weighted spin-echo imaging data (1 mm isotropic voxel) were also acquired for anatomical overlay.

We preprocessed the imaging following the workflows proposed in a previous paper[47]. All functional MR images were preprocessed using Analysis of Functional Neuroimages (Version AFNI_18.2.03) software[48]. All fMRI data were corrected for temporal shifts between slices and motion and grand-mean scaled. Low-frequency signal drifts were filtered using a cutoff of 128 s. Volumes meeting the following criteria were removed: translation>0.3mm or rotation>0.3° between consecutive volumes[49]. For each run, we dropped the first two volumes to enhance stability. Linear regression was also performed to remove linear trends. All functional volumes were non-linearly transformed to MNI space (resampled voxel size: $4 \times 4 \times 4$ mm^3) according to the spatial transformation between the anatomical data and the MNI space. Volumes were spatially smoothed with a Gaussian kernel (full-width at half-maximum = 8 mm) and were used for general linear model and psycho-physiological interaction (PPI) analysis. Unsmoothed data were used for MVPA.

General linear model for value signals. To illustrate the neural activations of the values, including RPE, gain, loss, and reward predictions for the four decks, a general linear model was used to examine the BOLD signals in which brain regions were correlated with these values. The general linear model was run for each value and included 1) an interest regressor, *i.e.*, one-value regressor, defined as RPE, gain, loss, or reward prediction for the four decks during the epochs when feedback was presented and 0 for

other epochs, and 2) six noninterest regressors for head motion. Then, the parameter estimates were extracted for each value and for each participant. We performed a group-level one-sample t test for parameter estimates using family-wise error correction.

Whole brain searchlight-based multivoxel pattern analysis. We first used whole brain searchlight-based MVPA to classify advantageous choice versus disadvantageous choice. We adapted the within-subject MVPA methods from a previous study[50]. We used the least squares-separate (LSS) method to extract choice-related activations according to a previous study[51]. LSS is the most effective method to estimate choice activation[51] and has been widely used in the field[50,52,53]. According to the LSS method, a general linear model was used to extract activation for each choice. There were 180 choices, $C_{1\ldots180}$, including advantageous choices and disadvantageous choices, for each participant. A general linear model was run for each choice. For the ith choice, C_i, the general linear model included two choice regressors. The first was the choice regressor of interest. During a trial with choice C_i, this regressor was defined as 1 during the epoch when a button press was made in the selection phase and 0 for the other epochs; during trials with choices $C_{1\ldots i-1,i+1\ldots180}$, this regressor was defined as 0 for all epochs. The other was the choice regressor of nuisance. During a trial with choice C_i, this regressor was defined as 0 for all epochs; during trials with choices $C_{1\ldots i-1,i+1\ldots180}$, this regressor was defined as 1 during the epoch when a button press was made in the selection phase and 0 for the other epochs. The value of β for the choice regressor of interest in the general linear model was the activation for choice C_i. The general linear model was repeated 180 times to extract activations for 180 choices for each participant. The general linear model was performed using MATLAB's *regstats* function (MATLAB v2019a, Mathworks Inc, Natick, MA, PC).

We implemented two steps to control the effects of values, as choices can be expected to be related to value signals, including RPE, gain, loss, and reward predictions for the four decks. For step 1, we used the Gram-Schmidt orthogonalization algorithm to orthogonalize choices and values before implementing the general linear model [54,55]. Specifically, we orthogonalized choice and RPE, gain, loss, and reward predictions for the four decks. For step 2, the orthogonalized choice regressor of interest, the orthogonalized choice regressor of nuisance, the regressors for RPE, gain, loss, and reward predictions for the four decks [those defined as RPE, gain, loss, or reward predictions for the four decks

during the epochs when feedback was presented and 0 for the other epochs], and six regressors of no interest for head motion were included in each general linear model. We extracted β, the activation of the orthogonalized choice regressor of interest, for each voxel in the whole brain in each general linear model. The extracted activations were grouped into two categories according to the choice type, i.e., advantageous choice versus disadvantageous choice, for each voxel and for each participant.

We performed whole brain searchlight-based MVPA that did not depend on a priori assumptions but searched for predictive information across the whole brain. For each voxel v_i, considering the local patterns that contained the spatial correlation that might decode advantageous choice versus disadvantageous choice, we constructed a spherical collection of voxels ($S_{I\ldots N}$), with 33 voxels[56] centred on voxel v_i. For each voxel $S_{I\ldots N}$ in the collection, we extracted β; namely, $V_{I\ldots N}$. $V_{I\ldots N}$ were normalized to the range from 0 to 1 for advantageous choice and disadvantageous choice separately to give all voxels equal importance during classifier training[57,58]. The values $V_{I\ldots N}$ were then used to train and test the classifier model, which was a support vector machine with a linear kernel. The decoding accuracy of the central voxel v_i was acquired by five-fold cross-validation. The implementation of the support vector machine and cross-validation were based on *sklearn.svm.SVC* in Python's scikit-learn toolbox (version 0.21.2)[59]. During training and testing of the classification model, random undersampling was used to handle the imbalance in samples between advantageous choice and disadvantageous choice. For example, if the number of advantageous choices was larger than that of disadvantageous choices, advantageous choices were removed randomly to make the numbers the same as the disadvantageous choices by the numpy.random.shuffle function in Python (version 3.6.8). Equal numbers of both choices were labelled the original data sample, which was then randomly partitioned into five equal sized subsamples for five-fold cross-validation. The same procedure was performed for each voxel over the whole brain for each participant. The whole brain decoding accuracy was normalized by subtracting the mean of the whole brain accuracy for each participant.

We performed a group-level one-sample t test for whole brain searchlight-based MVPA for decoding accuracy using family-wise error correction.

We also tested whether choice-related activations were correlated with value signals, i.e., RPE, gain,

loss, and reward predictions for the four decks using both whole brain analysis and region of interest (ROI) analysis. Specifically, the extracted activations in the general linear model were grouped into two categories according to the median split of the values of the trials, i.e., high and low subgroups for RPE, gain, loss, and reward predictions for the four decks for each participant. We tested whether these subgroups showed differences for RPE, reward predictions for the four decks, gain, and loss separately using the t test in the whole brain with family-wise error correction. We further included the left and right OFC ROIs from the Anatomical Automatic Labeling atlas (AAL2)[60]. The left OFC ROI included OFCmed_L, OFCant_L, OFCpost_L, and OFClat_L and the right OFC ROI included OFCmed_R, OFCant_R, OFCpost_R, and OFClat_R. The extracted activations for values above were averaged in the left and right OFC ROIs separately, then, were fed into group comparisons using the t test with uncorrected $p<0.05$.

ROI-based MVPA. We further tested whether the OFC represented choice using ROI-based MVPA. First, we included OFC ROIs from the AAL2 that showed overlapping areas with the peak voxel for significant clusters in the whole brain searchlight-based MVPA. Second, we extracted the activations associated with each choice for each OFC ROI. Activations were also normalized to the range from 0 to 1 for advantageous choice and disadvantageous choice separately[57,58]. The decoding accuracy for each OFC ROI was acquired by five-fold cross-validation.

We tested whether the decoding accuracy was greater than chance level (0.5) for each OFC ROI using a one-sample t test. We tested whether the decoding accuracy was correlated with the learning rate, total score, and total net good decks using Pearson correlations.

To test whether the signal-to-noise ratio (SNR) affected the decoding results, Pearson correlations between the SNR and decoding accuracy for each ROI were determined.

PPI analysis. To investigate whether the functional connectivity of the OFC identified in ROI-based MVPA differed between advantageous and disadvantageous choices, we ran PPI analysis. First, we created a "seed" time series by extracting mean time courses for each OFC identified in ROI-based MVPA. Second, we computed the interaction terms between the "seed" and either the (1) advantageous

choice regressor, defined as 1 during the epoch when a button press was made in the selection phase and 0 for other epochs during trials with advantageous choice and as 0 for all epochs during trials with disadvantageous choice or the (2) disadvantageous choice regressor, defined as 1 during the epoch when a button press was made in the selection phase and 0 for other epochs during trials with disadvantageous choice and as 0 for all epochs during trials with advantageous choice. Third, we estimated a PPI general linear model including the following regressors: (1) the advantageous choice regressor, (2) the disadvantageous choice regressor, (3) the OFC seed time course, (4) the interaction term between the "seed" and advantageous choice regressor, defined as advantageous choice PPI, (5) the interaction term between the "seed" and disadvantageous choice regressor, defined as disadvantageous choice PPI, (6) seven value regressors including RPE, gain, loss, and reward predictions for the four decks, defined as RPE, gain, loss, or reward predictions for the four decks, respectively, during the epochs when feedback was presented and 0 for the other epochs, and (7) six noninterest regressors for head motion. The PPI general linear model was performed using AFNI's *3dDeconvolve*.

We computed the first-level contrast for the disadvantageous choice PPI β minus the advantageous choice PPI β. We performed a one-sample t test to identify significant differences in the contrast to identify PPI effects using family-wise error correction.

We also tested whether there were overlapping regions in the brain among the whole brain searchlight-based MVPA and PPI.

As a control analysis, we tested whether value signals modulated OFC functional connectivity. To achieve this, we performed PPI analysis for RPE, gain, loss, and reward predictions for the four decks separately. The PPI general linear model included the following regressors: (1) a value regressor, defined as RPE, gain, loss, or reward predictions for the four decks during the epochs when feedback was presented and 0 for other epochs, (2) the OFC seed time course, (3) the interaction term between the "seed" and value regressor, defined as the value PPI, and (4) six noninterest regressors for head motion. We computed the first-level contrast for PPI β values and performed a one-sample t test to identify PPI effects using family-wise error correction.

Results

Summary of behavioural performance in the IGT

We found that the participants' learning rate was significantly higher than the learning rate from the computer's random 1000 selections [Mann-Whitney test, Mann-Whitney U=53, $p < .001$, 95% confidence interval: [0.085, 0.116]]. The participants' learning rate, response time, number of advantageous choices, number of disadvantageous choices, total score, and total net good decks are summarized in Table 1.

BOLD activity in the OFC is correlated with value signals

We found significant activations in the OFC, striatum, and posterior cingulate cortex for value signals, including RPE, gain, loss (Fig. 2 and Table 2), and reward predictions for the four decks (Supplementary Figure 1 and Supplementary Table 1). Therefore, the results are consistent with previous studies showing that the OFC is implicated in value evaluation[42,61,62].

The OFC represents advantageous choice

As the OFC has been implicated in the representation of value signals, we next examined whether the OFC represented advantageous choice while controlling for value effects. Using whole brain searchlight-based MVPA, we found that the activity pattern in the OFC indeed represented advantageous choice (Fig. 3a and Table 3). Whole brain searchlight-based MVPA also revealed that activity in the frontal regions and the parietal regions represented advantageous choice (Fig. 3a and Table 3); thus, we replicated similar findings regarding the representation of choice in the frontoparietal network from previous studies[1,2].

Are choice related activations in the OFC related to value signals? We found that there were no significant activations in the OFC between the high and low subgroups for RPE, gain, loss (Fig. 3b, 3c, 3d, and Supplementary Table 3), or reward predictions for the four decks (Supplementary Figure 2 and Supplementary Table 4). We further found that there were no significant differences in the left or right OFC ROIs between the high and low subgroups for RPE, gain, loss (all $p_s > 0.05, \text{uncorrected}$). The results suggest that choice-related activations in the OFC for MVPA were not confounded by value signals.

The peak voxels of significant clusters in the whole brain searchlight-based MVPA showed an overlapping area with OFCmed_R in AAL2; therefore, we further examined the choice representation in OFCmed_R using ROI-based MVPA. We found that OFCmed_R represented an advantageous choice [$t_{53} = 7.770, p < 0.001, Cohen's\ d = 1.057$, 95% confidence interval: [0.075, 0.126]] (Fig. 4a). We found significant correlations between the decoding accuracy and learning rate [$\mathrm{r} = 0.559, p < 0.001, \mathrm{N} = 54$], total score [$\mathrm{r} = 0.357, p = 0.008, \mathrm{N} = 54$], and total net good decks [$\mathrm{r} = 0.468, p < 0.001, \mathrm{N} = 54$] (Fig. 4b, 4c, and 4d). The decoding accuracy showed no significant correlations with the SNR [$\mathrm{r} = -0.119, p = 0.390, \mathrm{N} = 54$] or censor rate [$\mathrm{r} = 0.071, p = 0.610, \mathrm{N} = 54$], suggesting that the decoding accuracy was not explained by either of these parameters.

Choice modulates OFC functional connectivity with the superior medial gyrus

PPI analysis revealed greater OFC connectivity with the superior medial gyrus when choosing disadvantageous options versus choosing advantageous options (Fig. 5a). Furthermore, the superior medial gyrus showed an overlapping area with brain regions representing advantageous choice revealed by whole brain searchlight-based MVPA (Fig. 5b). As a control analysis, we tested whether value signals modulated OFC functional connectivity. We found that there was no significant OFC functional connectivity in the whole brain for RPE, gain, loss, or reward predictions for the four decks (Fig. 5c), suggesting that choice-modulated OFC functional connectivity was not confounded by the value signals.

Discussion

Consistent with the proposal of a good-based model, the present study demonstrates that the OFC represents advantageous choice, which provides strong evidence to support the role of the OFC in binary choice in the IGT. Furthermore, IGT behavioural performances were correlated with the advantageous choice representation in the OFC. Third, the functional connectivity between the OFC and superior medial gyrus supports choice.

The OFC represents an advantageous choice in the IGT

In the present study, we demonstrated that the OFC represents binary choice in the IGT based on the distributed activity pattern. These results are supported by neurobiological studies with human[14,63] as well as animal[64,65] prefrontal lesions (including in the OFC), consistently indicating that the OFC plays a necessary role in decision-making.

Furthermore, beyond the OFC, the frontoparietal network was also implicated in choice in the present study, and the finding is consistent with previous studies[1,2]. Both the OFC and the frontoparietal network represented choice in the present study; therefore, we expected to find functional connectivity between the regions for choice. Indeed, we identified a functional connectivity between the OFC and the superior medial gyrus for choice, but not for values, suggesting that the OFC is functionally coupled with the prefrontal cortex when humans make choices. As the frontoparietal network has been widely implicated various decision-making situations[1,2], the connectivity between the OFC and the superior medial gyrus would be helpful for choice under various decision-making contexts. We also found that OFC activity is related to value signals, e.g., RPE, gain, and loss. Therefore, the finding that both choice and value

were represented in the OFC may make it easier for individuals to make optimal choices with the help of frontoparietal network modulation during difficult decision-making situations that lack sufficient information.

A proposed role for the OFC: representation of choice-related complex information along a continuous spectrum

In the present study, the OFC was shown to represent advantageous choice. This finding is supported by a recently proposed cognitive map representing a state space[66]. In the context of the cognitive map, the OFC is activated when the decision maker becomes cognizant of unobservable information and makes a correct choice; however, the OFC would not activate when the decision maker is not cognizant of unobservable information and makes an incorrect choice[67].

Interestingly, in the present study, even though the participants did not know the specific reward value for each deck, the OFC nevertheless represented advantageous choice. Integration of these findings shows that exact knowledge of complex information is not necessary for OFC activation. This may suggest that the OFC, in part, could play a role in unconscious influences, e.g., emotions, in complex decision-making[68].

We found that decoding accuracy in the OFC correlated with decision-making performance. We therefore propose a role for the human OFC based on the cognitive map idea: the OFC may represent choice-related complex information along a continuum, e.g., from a high decoding accuracy of advantageous choice if the decision maker exactly knows the complex information to a low decoding

accuracy if they do not. Our proposal further predicts that the OFC represents choice in choosing between other decision-making parameters, such as self-control and cost. This is important because humans often face choices that have unknown costs for effort control. It is beneficial to exert an appropriate level of effort for an appropriate choice. The OFC seems to be a candidate for the brain region used when making choices based on the aforementioned parameters in a complex context; this hypothesis should be investigated in future work.

Several shortcomings of the present study should be acknowledged. First, few female participants were recruited in the present study. We conducted ROI-based MVPA for males and females separately to test whether females and males showed a difference in decoding accuracy. We found consistent results (see Supplementary Table 5) between the sexes, suggesting that the percentage of females might not influence our results. Future work should include more female participants to substantiate our conclusion. Second, the IGT design convolves decision-making with uncertainty with learning. Good learning would presumably result in choosing from the high value deck and not from the other decks and would also presumably result in choosing from the high value deck more in the late IGT runs and less in the early IGT runs. Therefore, a reasonable assumption would be that changes in activation patterns between choosing high value versus choosing low value may be due to differences in choice probability. However, the choice probability is related to reward prediction, which we controlled for when we performed MVPA and PPI analysis. We found that choice-related activations in the OFC could represent choice in MVPA and that choice-related activations in the OFC were not related to reward predictions. We also found that choice, but not reward predictions, modulated OFC functional connectivity with the superior medial gyrus in PPI analysis. Therefore, our results suggest that neither

417 the choice probability nor the learning effect in the IGT confounds the decoding or PPI results in the
418 present study. Future work will require a complex decision-making task without learning to substantiate
419 our conclusion. Third, attention modulates the value signal in the OFC[69], thus, a reasonable assumption
420 would be that choice-related signals in the OFC may be confounded with attention. However, the OFC
421 signal has been related to value of attended option[69] and we found that choice-related signals in the OFC
422 were not related to all value signals, including RPE, gain, loss, or reward predictions for the four decks.
423 Therefore, our results suggest that attention may not confound the decoding or PPI results in the present
424 study. Future work will require a decision-making task with covert shift of attention to substantiate our
425 conclusion.
426
427 **Conclusions**
428 In conclusion, our results demonstrate that the OFC represents advantageous choice in the IGT. Our
429 data provide evidence to support the integration of knowledge in the OFC to make choices in a complex
430 context, which may be helpful for survival. Decreased decoding accuracy in the OFC may be related to
431 poor decision-making ability, and these findings may provide potential insight into understanding
432 impulsive behaviours.

Credit authorship contribution statement

Rujing Zha: Conceptualization, Formal analysis, Methodology, Software, Data curation, Writing-Original draft preparation, Project administration; Peng Li: Data curation, Formal analysis, Methodology, Writing-Reviewing and Editing; Ying Li: Formal analysis, Validation, Visualization; Nan Li: Formal analysis; Meijun Gao: Formal analysis, Writing- Reviewing and Editing; Yiyang Fan: Formal analysis; Ruhuiya Aili: Formal analysis; Ying Liu: Methodology; Xiaochu Zhang: Supervision, Conceptualization, Methodology, Writing-Reviewing and Editing; Jun Li: Supervision, Conceptualization, Methodology, Writing-Reviewing and Editing.

Data availability

All data are available from the authors.

Code availability

Matlab codes are available from the authors. Code for fMRI orthogonalization are available at https://www.mathworks.com/matlabcentral/fileexchange/55881-gram-schmidt-orthogonalization. Code for MVPA analysis are available at https://scikit-learn.org/dev/modules/svm.html#svm-classification. Code for PPI analysis are available at https://afni.nimh.nih.gov/CD-CorrAna.

Acknowledgements:

A portion of the numerical calculations in this study were performed with the supercomputing system at the Supercomputing Centre of USTC. We also thank the Bioinformatics Center of the University of Science and Technology of China, School of Life Science, for providing supercomputing resources for this project. We

455 would also like to acknowledge the professional manuscript services of SpringerNature Author Services.
456 This work was supported by grants from The National Key Basic Research Program (2018YFC0831101),
457 The National Natural Science Foundation of China (31471071, 31771221, 61773360, and 71874170), The
458 Fundamental Research Funds for the Central Universities of China.

459

460 **Declarations of interest:** none

461

References

1 Kable, J. W. & Glimcher, P. W. The neurobiology of decision: consensus and controversy. *Neuron* **63**, 733-745, doi:10.1016/j.neuron.2009.09.003 (2009).

2 Hunt, L. T., Dolan, R. J. & Rehrens, T. E. J. Hierarchical competitions subserving multi-attribute choice. *Nature neuroscience* **17**, 1613-1622, doi:10.1038/nn.3836 (2014).

3 Rodriguez, C. A., Turner, B. M. & McClure, S. M. Intertemporal Choice as Discounted Value Accumulation. *PloS one* **9**, 9, doi:10.1371/journal.pone.0090138 (2014).

4 Padoa-Schioppa, C. in *Neurobiology of Economic Choice: A Good-Based Model* Vol. 34 *Annual Review of Neuroscience* (eds S. E. Hyman *et al.*) 333-359 (2011).

5 Padoa-Schioppa, C. & Assad, J. A. Neurons in the orbitofrontal cortex encode economic value. *Nature* **441**, 223-226, doi:10.1038/nature04676 (2006).

6 Cai, X. & Padoa-Schioppa, C. Neuronal evidence for good-based economic decisions under variable action costs. *Nature Communications* **10**, doi:10.1038/s41467-018-08209-3 (2019).

7 Raghuraman, A. P. & Padoa-Schioppa, C. Integration of Multiple Determinants in the Neuronal Computation of Economic Values. *Journal of Neuroscience* **34**, 11583-11603, doi:10.1523/jneurosci.1235-14.2014 (2014).

8 Chen, Z., Guo, Y., Zhang, S. & Feng, T. Pattern classification differentiates decision of intertemporal choices using multi-voxel pattern analysis. *Cortex* **111**, 183-195, doi:10.1016/j.cortex.2018.11.001 (2019).

9 Linhartova, P. *et al.* Impulsivity in patients with borderline personality disorder: a comprehensive profile compared with healthy people and patients with ADHD. *Psychological medicine* **50**, 1829-1838, doi:10.1017/s0033291719001892 (2020).

10 Verharen, J. P. H. *et al.* Insensitivity to Losses: A Core Feature in Patients With Anorexia Nervosa? *Biol. Psychiat.-Cogn. Neurosci. Neuroimag.* **4**, 995-1003, doi:10.1016/j.bpsc.2019.05.001 (2019).

11 Kluwe-Schiavon, B. *et al.* Substance related disorders are associated with impaired valuation of delayed gratification and feedback processing: A multilevel meta-analysis and meta-regression. *Neuroscience and biobehavioral reviews* **108**, 295-307, doi:10.1016/j.neubiorev.2019.11.016 (2020).

12 Nistico, V., De Angelis, A., Erro, R., Demartini, B. & Ricciardi, L. Obsessive-Compulsive Disorder and Decision Making under Ambiguity: A Systematic Review with Meta-Analysis. *Brain sciences* **11**, 20, doi:10.3390/brainsci11020143 (2021).

13 Betz, L. T. *et al.* Deciphering reward-based decision-making in schizophrenia: A meta-analysis and behavioral modeling of the Iowa Gambling Task. *Schizophr. Res.* **204**, 7-15, doi:10.1016/j.schres.2018.09.009 (2019).

14 Bechara, A., Damasio, H., Tranel, D. & Damasio, A. R. Deciding advantageously before knowing the advantageous strategy. *Science* **275**, 1293-1295 (1997).

15 Stuphorn, V. Decision Making: How Is Information Represented in Orbitofrontal Cortex? *Curr. Biol.* **30**, R35-R37, doi:10.1016/j.cub.2019.11.015 (2020).

16 Yamada, H., Louie, K., Tymula, A. & Glimcher, P. W. Free choice shapes normalized value signals in medial orbitofrontal cortex. *Nature Communications* **9**, 11, doi:10.1038/s41467-017-02614-w (2018).

17 Malvaez, M., Shieh, C., Murphy, M. D., Greenfield, V. Y. & Wassum, K. M. Distinct cortical-amygdala projections drive reward value encoding and retrieval. *Nature neuroscience* **22**, 762-+, doi:10.1038/s41593-019-0374-7 (2019).

18 Ballesta, S., Shi, W., Conen, K. E. & Padoa-Schioppa, C. Values encoded in orbitofrontal cortex are

causally related to economic choices. *Nature* **588**, 450-+, doi:10.1038/s41586-020-2880-x (2020).
19 Preuschoff, K., Quartz, S. R. & Bossaerts, P. Human insula activation reflects risk prediction errors as well as risk. *Journal of Neuroscience* **28**, 2745-2752, doi:10.1523/jneurosci.4286-07.2008 (2008).
20 Payzan-LeNestour, E., Dunne, S., Bossaerts, P. & O'Doherty, J. P. The neural representation of unexpected uncertainty during value-based decision making. *Neuron* **79**, 191-201, doi:10.1016/j.neuron.2013.04.037 (2013).
21 Levy, I., Snell, J., Nelson, A. J., Rustichini, A. & Glimcher, P. W. Neural representation of subjective value under risk and ambiguity. *Journal of neurophysiology* **103**, 1036-1047, doi:10.1152/jn.00853.2009 (2010).
22 Hsu, M., Bhatt, M., Adolphs, R., Tranel, D. & Camerer, C. F. Neural systems responding to degrees of uncertainty in human decision-making. *Science* **310**, 1680-1683, doi:10.1126/science.1115327 (2005).
23 Vertechi, P. *et al.* Inference-Based Decisions in a Hidden State Foraging Task: Differential Contributions of Prefrontal Cortical Areas. *Neuron*, doi:10.1016/j.neuron.2020.01.017 (2020).
24 Hare, T. A., Camerer, C. F. & Rangel, A. Self-Control in Decision-Making Involves Modulation of the vmPFC Valuation System. *Science* **324**, 646-648, doi:10.1126/science.1168450 (2009).
25 Kable, J. W. & Glimcher, P. W. The neural correlates of subjective value during intertemporal choice. *Nature neuroscience* **10**, 1625-1633 (2007).
26 Clithero, J. A. & Rangel, A. Informatic parcellation of the network involved in the computation of subjective value. *Soc Cogn Affect Neurosci* **9**, 1289-1302, doi:10.1093/scan/nst106 (2014).
27 Bartra, O., McGuire, J. T. & Kable, J. W. The valuation system: A coordinate-based meta-analysis of BOLD fMRI experiments examining neural correlates of subjective value. *NeuroImage* **76**, 412-427, doi:10.1016/j.neuroimage.2013.02.063 (2013).
28 Huettel, S. A., Stowe, C. J., Gordon, E. M., Warner, B. T. & Platt, M. L. Neural signatures of economic preferences for risk and ambiguity. *Neuron* **49**, 765-775, doi:10.1016/j.neuron.2006.01.024 (2006).
29 Bach, D. R., Hulme, O., Penny, W. D. & Dolan, R. J. The known unknowns: neural representation of second-order uncertainty, and ambiguity. *The Journal of neuroscience : the official journal of the Society for Neuroscience* **31**, 4811-4820, doi:10.1523/JNEUROSCI.1452-10.2011 (2011).
30 Fukui, H., Murai, T., Fukuyama, H., Hayashi, T. & Hanakawa, T. Functional activity related to risk anticipation during performance of the Iowa Gambling Task. *NeuroImage* **24**, 253-259, doi:10.1016/j.neuroimage.2004.08.028 (2005).
31 Lin, C. H., Chiu, Y. C., Cheng, C. M. & Hsieh, J. C. Brain maps of Iowa gambling task. *BMC Neurosci* **9**, 72, doi:10.1186/1471-2202-9-72 (2008).
32 Lawrence, N. S., Jollant, F., O'Daly, O., Zelaya, F. & Phillips, M. L. Distinct roles of prefrontal cortical subregions in the Iowa Gambling Task. *Cerebral cortex* **19**, 1134-1143, doi:10.1093/cercor/bhn154 (2009).
33 Tanabe, J. *et al.* Prefrontal cortex activity is reduced in gambling and nongambling substance users during decision-making. *Human brain mapping* **28**, 1276-1286, doi:10.1002/hbm.20344 (2007).
34 Ma, S., Zang, Y., Cheung, V. & Chan, C. C. Importance of punishment frequency in the Iowa gambling task: an fMRI study. *Brain imaging and behavior* **9**, 899-909, doi:10.1007/s11682-015-9353-0 (2015).
35 Power, Y., Goodyear, B. & Crockford, D. Neural correlates of pathological gamblers preference for immediate rewards during the iowa gambling task: an fMRI study. *Journal of gambling studies / co-sponsored by the National Council on Problem Gambling and Institute for the Study of Gambling and Commercial Gaming* **28**, 623-636, doi:10.1007/s10899-011-9278-5 (2012).
36 Ding, Y. *et al.* Altered brain processing of decision-making in healthy first-degree biological relatives of

suicide completers. *Molecular psychiatry* **22**, 1149-1154, doi:10.1038/mp.2016.221 (2017).
37 Brevers, D., Noel, X., He, Q., Melrose, J. A. & Bechara, A. Increased ventral-striatal activity during monetary decision making is a marker of problem poker gambling severity. *Addiction biology* **21**, 688-699, doi:10.1111/adb.12239 (2016).
38 Werner, N. S. *et al.* Interoceptive awareness moderates neural activity during decision-making. *Biol Psychol* **94**, 498-506, doi:10.1016/j.biopsycho.2013.09.002 (2013).
39 Jollant, F. *et al.* Decreased activation of lateral orbitofrontal cortex during risky choices under uncertainty is associated with disadvantageous decision-making and suicidal behavior. *NeuroImage* **51**, 1275-1281, doi:10.1016/j.neuroimage.2010.03.027 (2010).
40 Christakou, A., Brammer, M., Giampietro, V. & Rubia, K. Right ventromedial and dorsolateral prefrontal cortices mediate adaptive decisions under ambiguity by integrating choice utility and outcome evaluation. *The Journal of neuroscience : the official journal of the Society for Neuroscience* **29**, 11020-11028, doi:10.1523/JNEUROSCI.1279-09.2009 (2009).
41 Norman, K. A., Polyn, S. M., Detre, G. J. & Haxby, J. V. Beyond mind-reading: multi-voxel pattern analysis of fMRI data. *Trends Cogn Sci* **10**, 424-430, doi:10.1016/j.tics.2006.07.005 (2006).
42 Wang, Y. *et al.* Neural substrates of updating the prediction through prediction error during decision making. *NeuroImage* **157**, 1-12, doi:10.1016/j.neuroimage.2017.05.041 (2017).
43 Wei, Z. *et al.* Chronic nicotine exposure impairs uncertainty modulation on reinforcement learning in anterior cingulate cortex and serotonin system. *Neuroimage* **169**, 323-333, doi:10.1016/j.neuroimage.2017.11.048 (2018).
44 Behrens, T. E., Woolrich, M. W., Walton, M. E. & Rushworth, M. F. Learning the value of information in an uncertain world. *Nature neuroscience* **10**, 1214-1221, doi:10.1038/nn1954 (2007).
45 Sutton, R. S. & Barto, A. G. Reinforcement Learning: An Introduction. (1998).
46 Faul, F., Erdfelder, E., Lang, A. G. & Buchner, A. G*Power 3: a flexible statistical power analysis program for the social, behavioral, and biomedical sciences. *Behav Res Methods* **39**, 175-191 (2007).
47 Esteban, O. *et al.* fMRIPrep: a robust preprocessing pipeline for functional MRI. *Nat. Methods* **16**, 111-+, doi:10.1038/s41592-018-0235-4 (2019).
48 Cox, R. W. AFNI: software for analysis and visualization of functional magnetic resonance neuroimages. *Computers and biomedical research, an international journal* **29**, 162-173 (1996).
49 Rose, E. J. *et al.* The NOS1 variant rs6490121 is associated with variation in prefrontal function and grey matter density in healthy individuals. *NeuroImage* **60**, 614-622, doi:10.1016/j.neuroimage.2011.12.054 (2012).
50 Zha, R. *et al.* Transforming brain signals related to value evaluation and self-control into behavioral choices. *Human brain mapping* **40**, 1049-1061, doi:10.1002/hbm.24379 (2019).
51 Mumford, J. A., Turner, B. O., Ashby, F. G. & Poldrack, R. A. Deconvolving BOLD activation in event-related designs for multivoxel pattern classification analyses. *NeuroImage* **59**, 2636-2643, doi:10.1016/j.neuroimage.2011.08.076 (2012).
52 Piva, M. *et al.* The dorsomedial prefrontal cortex computes task-invariant relative subjective value for self and other. *Elife* **8**, doi:10.7554/eLife.44939 (2019).
53 Corradi-Dell'Acqua, C., Tusche, A., Vuilleumier, P. & Singer, T. Cross-modal representations of first-hand and vicarious pain, disgust and fairness in insular and cingulate cortex. *Nat Commun* **7**, 10904, doi:10.1038/ncomms10904 (2016).
54 Pine, A. *et al.* Encoding of marginal utility across time in the human brain. *The Journal of neuroscience : the official journal of the Society for Neuroscience* **29**, 9575-9581,

doi:10.1523/JNEUROSCI.1126-09.2009 (2009).
55 Chen, M. Gram-Schmidt orthogonalization (https://www.mathworks.com/matlabcentral/fileexchange/55881-gram-schmidt-orthogonalization). *MATLAB Central File Exchange. Retrieved February 16* (2021).
56 Kriegeskorte, N., Goebel, R. & Bandettini, P. Information-based functional brain mapping. *Proc Natl Acad Sci U S A* **103**, 3863-3868, doi:10.1073/pnas.0600244103 (2006).
57 Linn, K. A. *et al.* Control-group feature normalization for multivariate pattern analysis of structural MRI data using the support vector machine. *NeuroImage* **132**, 157-166, doi:10.1016/j.neuroimage.2016.02.044 (2016).
58 Peng, X., Lin, P., Zhang, T. & Wang, J. Extreme learning machine-based classification of ADHD using brain structural MRI data. *PloS one* **8**, e79476, doi:10.1371/journal.pone.0079476 (2013).
59 Pedregosa, F. *et al.* Scikit-learn: Machine Learning in Python. *J. Mach. Learn. Res.* **12**, 2825-2830 (2011).
60 Rolls, E. T., Joliot, M. & Tzourio-Mazoyer, N. Implementation of a new parcellation of the orbitofrontal cortex in the automated anatomical labeling atlas. *NeuroImage* **122**, 1-5, doi:10.1016/j.neuroimage.2015.07.075 (2015).
61 Antony, J. W. *et al.* Behavioral, Physiological, and Neural Signatures of Surprise during Naturalistic Sports Viewing. *Neuron* **109**, 377-+, doi:10.1016/j.neuron.2020.10.029 (2021).
62 Tom, S. M., Fox, C. R., Trepel, C. & Poldrack, R. A. The neural basis of loss aversion in decision-making under risk. *Science* **315**, 515-518, doi:10.1126/science.1134239 (2007).
63 Manes, F. *et al.* Decision-making processes following damage to the prefrontal cortex. *Brain* **125**, 624-639 (2002).
64 Bradfield, L. A., Dezfouli, A., van Holstein, M., Chieng, B. & Balleine, B. W. Medial Orbitofrontal Cortex Mediates Outcome Retrieval in Partially Observable Task Situations. *Neuron* **88**, 1268-1280, doi:10.1016/j.neuron.2015.10.044 (2015).
65 Stolyarova, A. & Izquierdo, A. Complementary contributions of basolateral amygdala and orbitofrontal cortex to value learning under uncertainty. *Elife* **6**, doi:10.7554/eLife.27483 (2017).
66 Wilson, R. C., Takahashi, Y. K., Schoenbaum, G. & Niv, Y. Orbitofrontal cortex as a cognitive map of task space. *Neuron* **81**, 267-279, doi:10.1016/j.neuron.2013.11.005 (2014).
67 Schuck, N. W., Cai, M. B., Wilson, R. C. & Niv, Y. Human Orbitofrontal Cortex Represents a Cognitive Map of State Space. *Neuron* **91**, 1402-1412, doi:10.1016/j.neuron.2016.08.019 (2016).
68 Poppa, T. & Bechara, A. The somatic marker hypothesis: revisiting the role of the 'body-loop' in decision-making. *Current Opinion in Behavioral Sciences* **19**, 61-66, doi:10.1016/j.cobeha.2017.10.007 (2018).
69 Xie, Y., Nie, C. & Yang, T. Covert shift of attention modulates the value encoding in the orbitofrontal cortex. *Elife* **7**, doi:10.7554/eLife.31507 (2018).

632 **Figure Legends**

633 **Figure 1. Experimental paradigm of the Iowa gambling task.** Experimental paradigm of the Iowa
634 gambling task. There were two phases for each trial. Four decks were presented in the first phase. Participants
635 selected a card within 4 s in this phase (selection phase, 4 s); then, the outcome, including gain and loss, was
636 presented in the second phase (feedback phase, 1 s).

637 **Figure 2. BOLD activity in the OFC was correlated with value signals.** BOLD signals in the OFC,
638 striatum, and posterior cingulate cortex were correlated with value signals, including a) RPE, b) gain, and c)
639 loss. Family-wise error at a cluster-level threshold of $p < 0.05$ (voxel-level threshold of $p < 0.001$, voxel
640 size > 13 for RPE, 33 for gain, and 19 for loss). $N = 54$.

641 **Figure 3. The OFC represents advantageous choice, and choice-related activations in the OFC are not**
642 **correlated with value signals.** a) Whole brain searchlight-based MVPA revealed that the OFC represents
643 choice. Choice-related activations in the OFC are not significantly correlated with value signals, including
644 b) RPE, c) gain, or d) loss. R, Right, L, Left. Family-wise error at a cluster-level threshold of $p < 0.05$ (voxel-
645 level threshold of $p < 0.001$, voxel size > 4 for advantageous choice, 1 for RPE, 3 for gain, and 2 for loss).
646 $N = 54$.

647 **Figure 4. The OFC represents an advantageous choice, and the OFC decoding accuracy is correlated**
648 **with behavioural performances.** a) The OFCmed_R region in AAL2 represents an advantageous choice.
649 The OFCmed_R decoding accuracy was correlated with the b) learning rate, c) total score, and d) total net
650 good decks in the IGT. The dashed line in the panels shows the chance level (0.5), and the dashed area in
651 the panels shows the 95% confidence interval. The error bar shows SE. $N = 54$.

652

653 **Figure 5. The OFC is functionally connected with the superior medial gyrus for choice, but not for**

values. a) Compared with advantageous choice, disadvantageous choice increased the OFC functional connectivity with the superior medial gyrus. Voxel size: 40; peak voxel coordinates: -10, -66, +4. R, Right, L, Left. Family-wise error at a cluster-level threshold of $p < 0.05$ (voxel-level threshold of $p < 0.001$, voxel size > 13). b) The overlapping area between the superior medial gyrus and the brain regions representing advantageous choice contained 16 voxels. c) There was no significant OFC functional connectivity across the whole brain for RPE, gain, loss, or reward predictions for the four decks. Family-wise error at a cluster-level threshold of $p < 0.05$ (voxel-level threshold of $p < 0.001$, voxel size > 1 for RPE, 3 for gain, 2 for loss, 16 for reward prediction for deck A, 18 for reward prediction for deck B, 16 for reward prediction for deck C, 15 for reward prediction for deck D). $N = 54$.

665 **Table Legends**

666 **Table 1. Summary of behavioural performance in the Iowa gambling task.**

667 *N* = 54.

668 **Table 2. BOLD activity in the OFC is correlated with the value signals.**

669 [a] The coordinates of the peak voxel are shown in MNI space (+ left, - right; + posterior, - anterior; + superior,

670 - inferior). Family-wise error at a cluster-level threshold of $p < 0.05$ (voxel-level threshold of $p < 0.001$,

671 voxel size > 13 for RPE, 33 for gain, and 19 for loss). *N* = 54.

672 **Table 3. Brain regions including the OFC that represent advantageous choice**.

673 [a] The coordinates of the peak voxel are shown in MNI space (+ left, - right; + posterior, - anterior; + superior,

674 - inferior). Family-wise error at a cluster-level threshold of $p < 0.05$ (voxel-level threshold of $p < 0.001$,

675 voxel size > 4). This table only displays the brain regions that formed a cluster of more than 20 voxels; all

676 significant clusters are shown in Supplementary Table 2. *N* = 54.

677

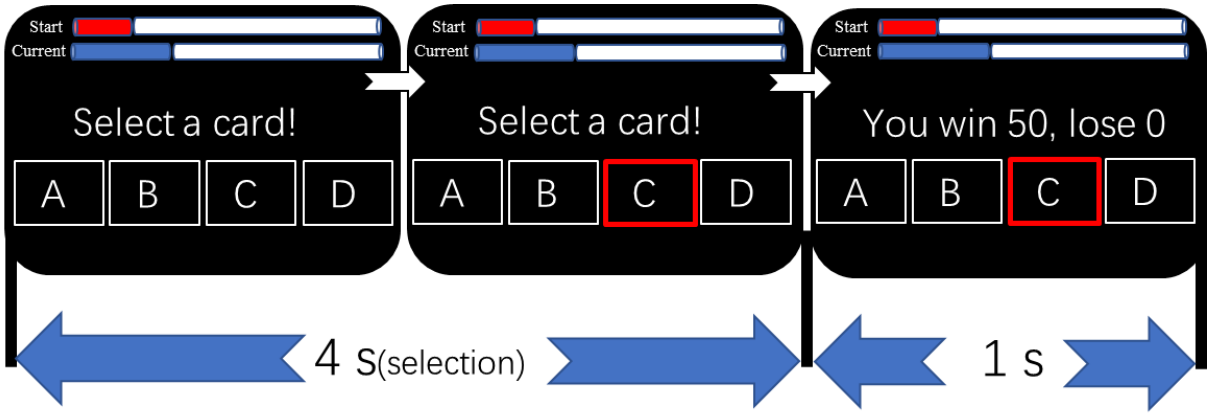

678

679 **Figure 1. Experimental paradigm of the Iowa gambling task.**

680

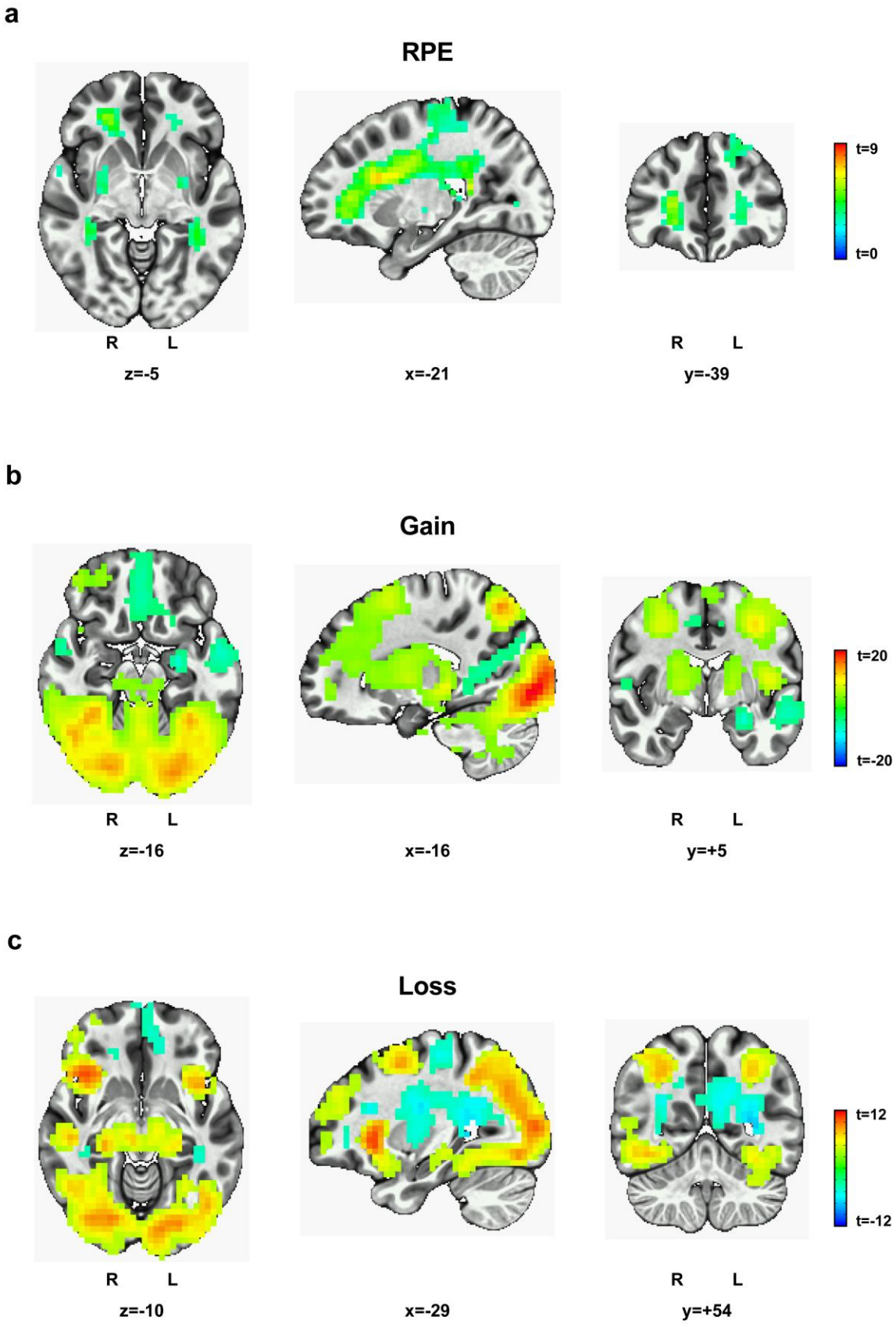

Figure 2. BOLD activity in the OFC was correlated with value signals.

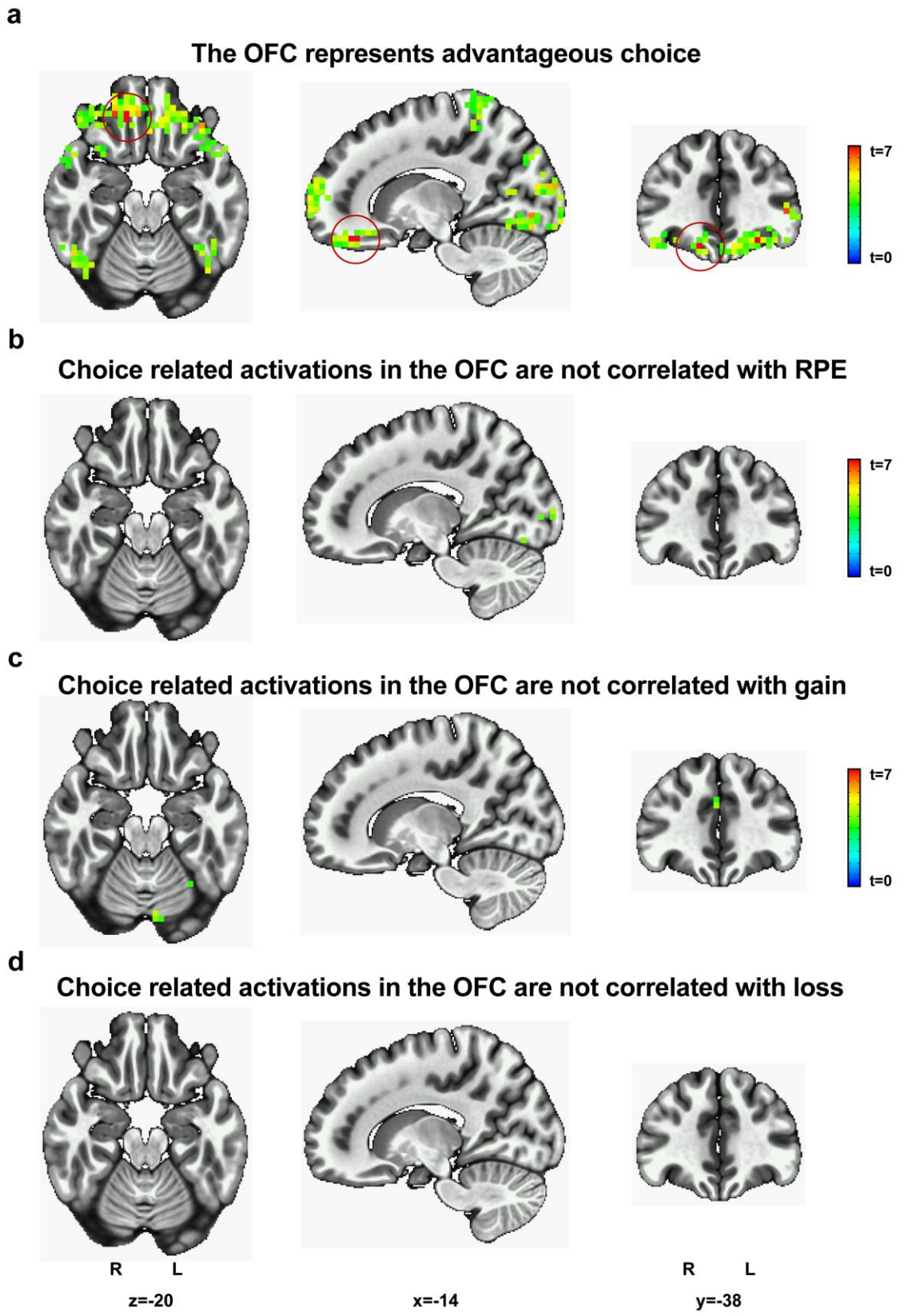

684

685 **Figure 3. The OFC represents advantageous choice, and choice-related activations in the OFC are**
686 **not correlated with value signals.**

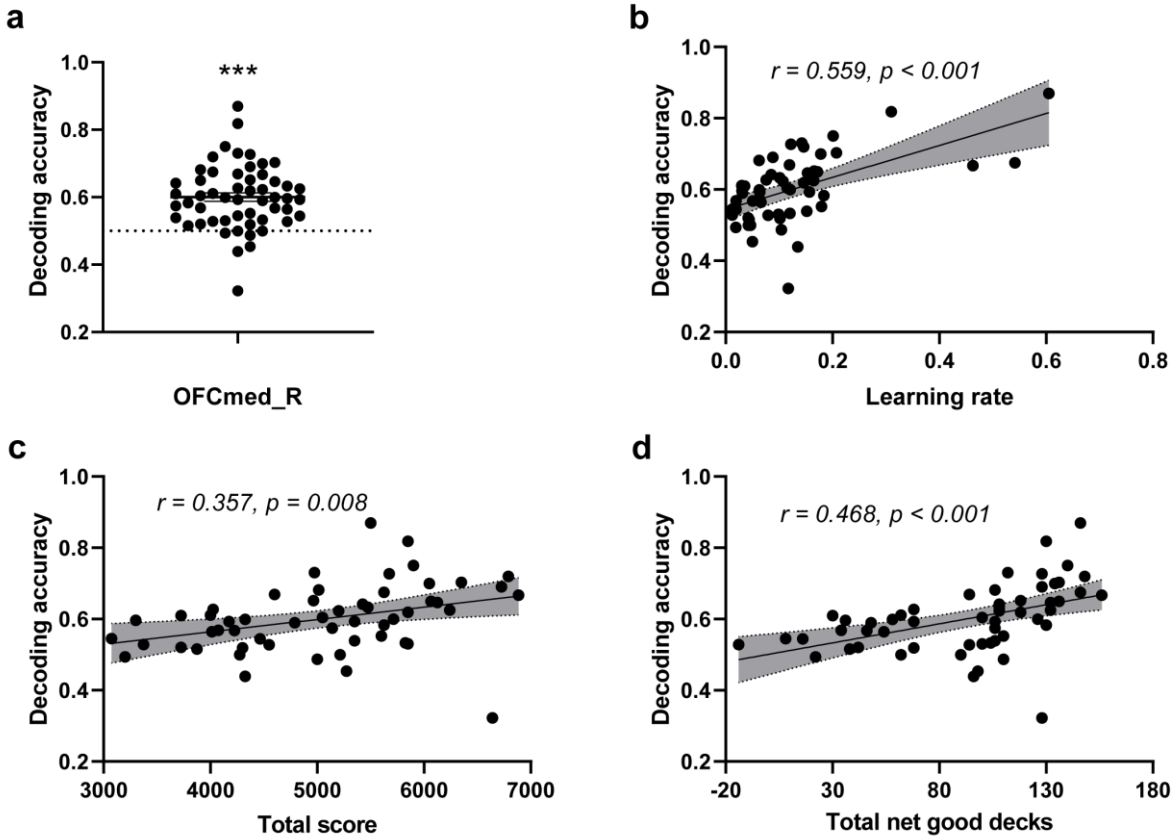

687

688 **Figure 4. The OFC represents an advantageous choice, and the OFC decoding accuracy is correlated**
689 **with behavioural performances.**

690

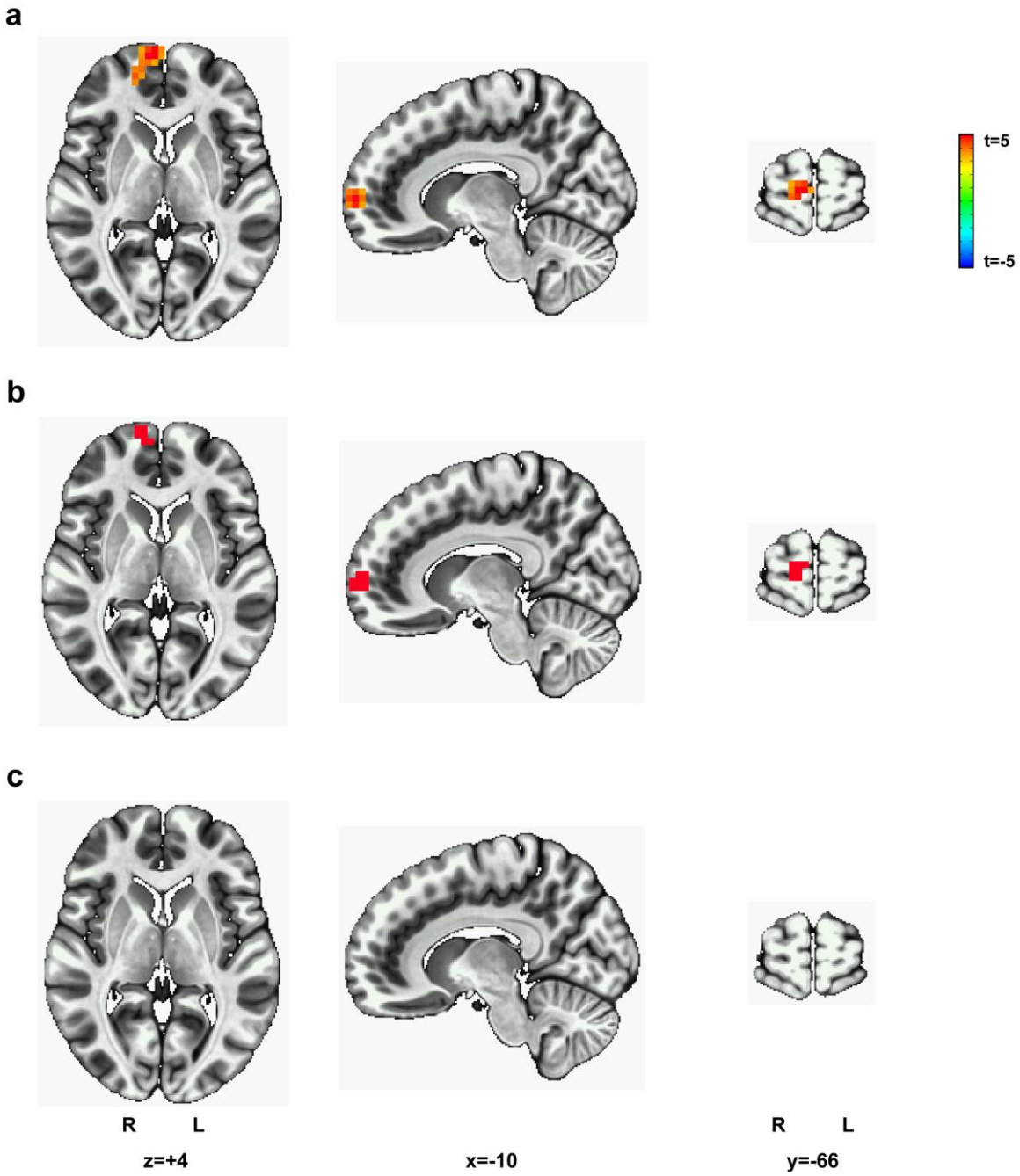

Figure 5. The OFC is functionally connected with the superior medial gyrus for choice, but not for values.

Table 1. Summary of behavioural performance in the Iowa gambling task.

	Mean	SD	Min	Max
Learning rate	0.152	0.119	0.012	0.605
Response time	0.655	0.240	0.273	1.424
The number of advantageous choices	136.426	20.752	83.000	168.000
The number of disadvantageous choices	43.574	20.752	12.000	97.000
Total score	5050.741	977.772	3075	6885
Total net good decks	92.852	41.503	-14.000	156.000

698 **Table 2.** BOLD activity in the OFC is correlated with the value signals.

	Brain regions	Voxels	x[a]	y	z
RPE	Right inferior frontal gyrus	2450	-26	-22	+24
	Left superior frontal gyrus	43	+22	-42	+48
	Left superior frontal gyrus	37	+18	-62	+12
	Right cerebellum	20	-42	+78	-36
	Left cerebellum	19	+10	+46	-16
Gain	Right lingual gyrus	11827	-18	+90	-4
	Left hippocampus	337	+26	+10	-16
	Left mid orbital gyrus	301	+2	-54	-12
	Right medial temporal pole	124	-50	-14	-28
	Right Rolandic operculum	80	-42	+14	+20
	Right SMA	75	-6	+10	+52
	Right angular gyrus	42	-58	+66	+28
Loss	Right insula lobe	4508	-34	-22	+0
	Right inferior parietal lobule	3604	-42	+42	+48
	Left paracentral lobule	531	+6	+30	+64
	Left middle frontal gyrus	65	+50	-38	+20
	Right cerebellum	28	-42	+82	-36
	Left superior frontal gyrus	25	+18	-46	+48

699

700

701 **Table 3. Brain regions including the OFC that represent advantageous choice**.

Brain regions	**Voxels**	**x**[a]	**y**	**z**
Right inferior occipital gyrus	497	-38	+82	-16
Right superior medial gyrus	157	-10	-66	+20
Left superior orbital gyrus	135	+14	-62	-8
Right superior orbital gyrus	130	-14	-38	-20
Left superior temporal gyrus	72	+54	+38	+20
Right middle temporal gyrus	59	-54	+38	+4
Left insula lobe	46	+42	-6	-12
Right paracentral lobule	45	-2	+38	+76
Right superior occipital gyrus	42	-30	+78	+40
Left inferior occipital gyrus	39	+46	+74	-8
Right temporal pole	36	-62	-2	+0
Right temporal pole	28	-54	-14	-16
Right angular gyrus	27	-50	+70	+36
Left superior parietal lobule	27	+22	+46	+64
Left superior parietal lobule	26	+30	+66	+64
Left inferior occipital gyrus	22	+18	+98	-8
Left temporal pole	20	+58	-10	-4
Left postcentral gyrus	20	+66	+14	+16

702

Figures

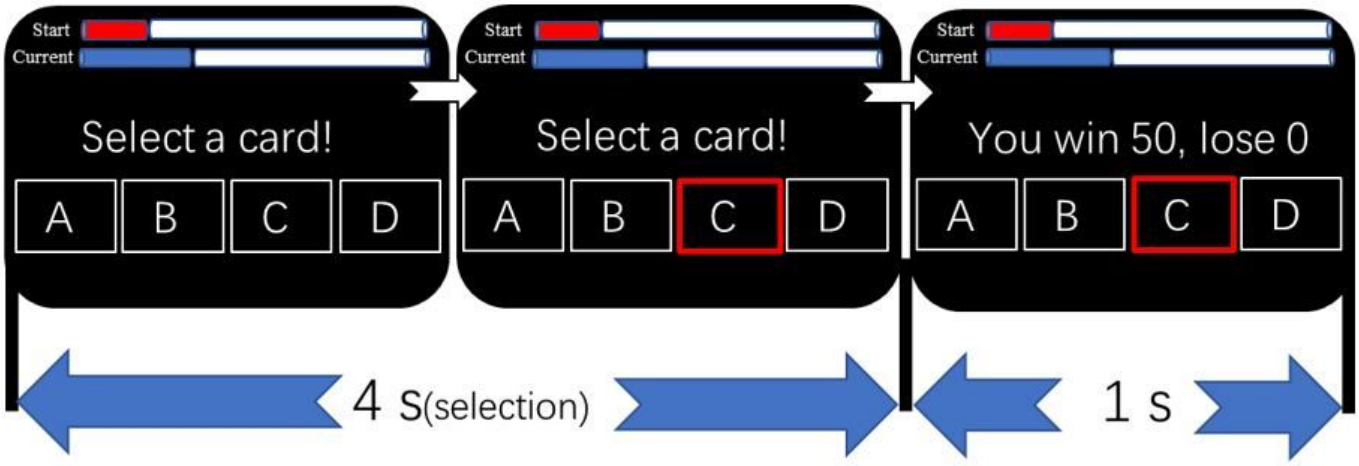

Figure 1

Experimental paradigm of the Iowa gambling task.

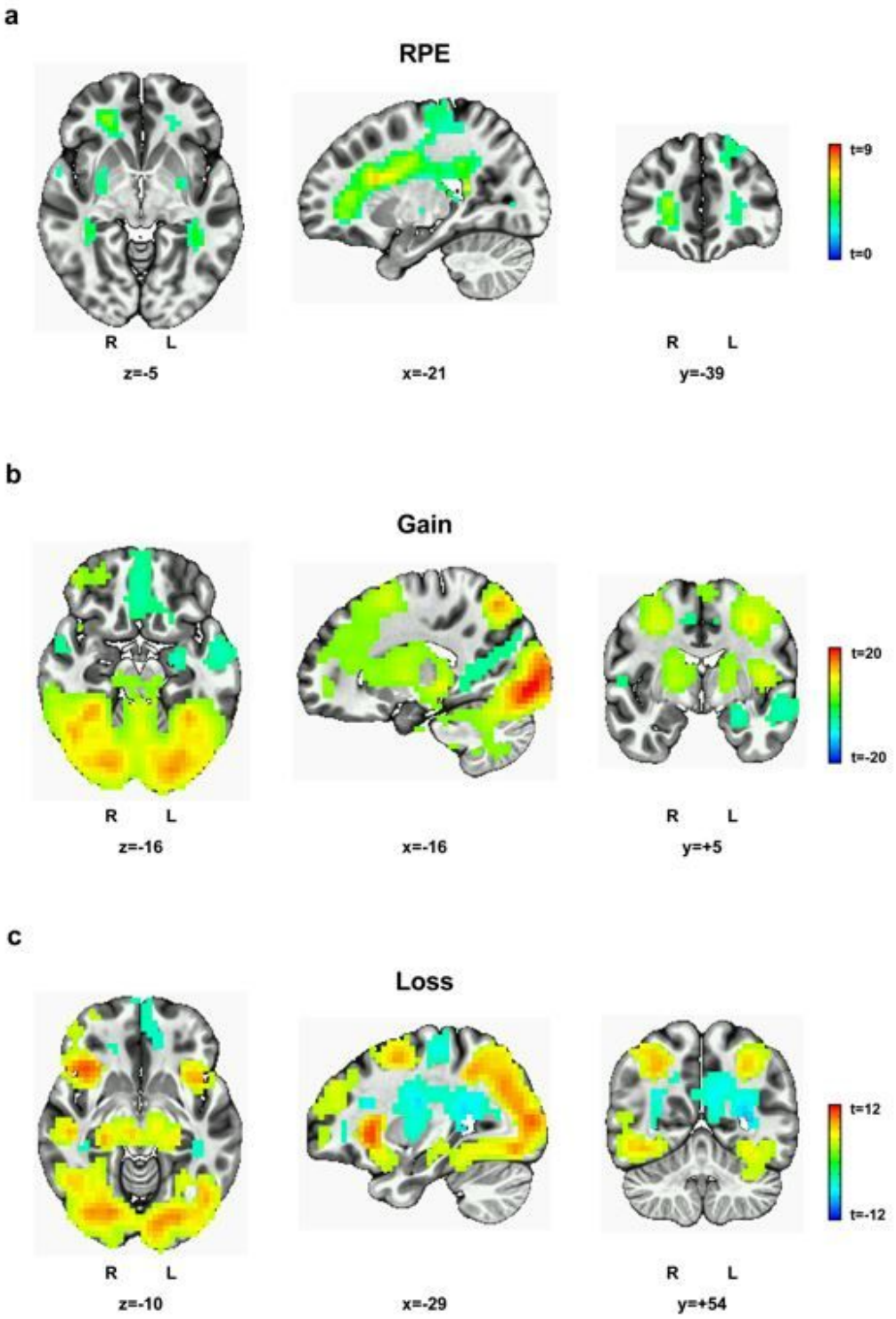

Figure 2

BOLD activity in the OFC was correlated with value signals.

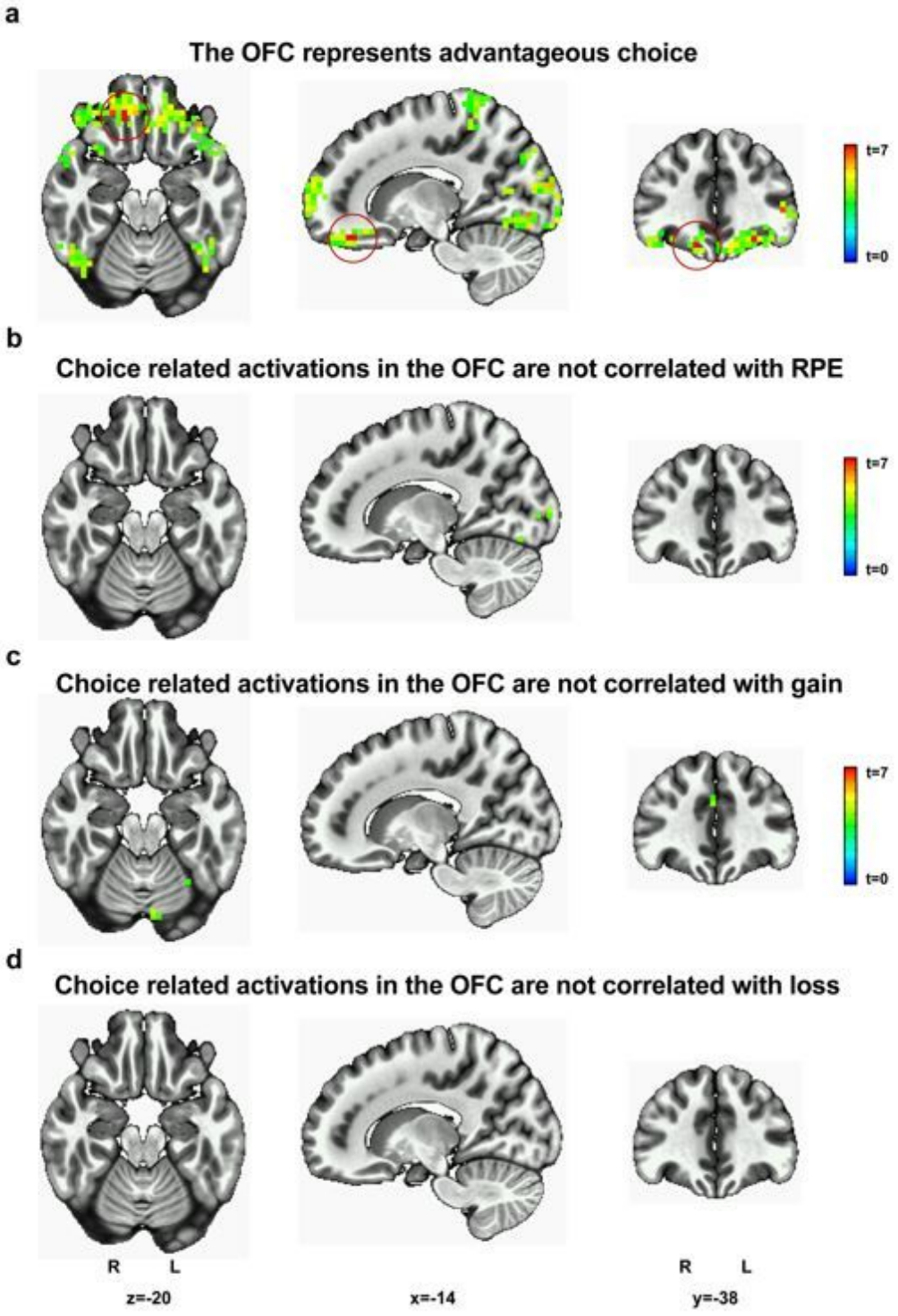

Figure 3

The OFC represents advantageous choice, and choice-related activations in the OFC are not correlated with value signals.

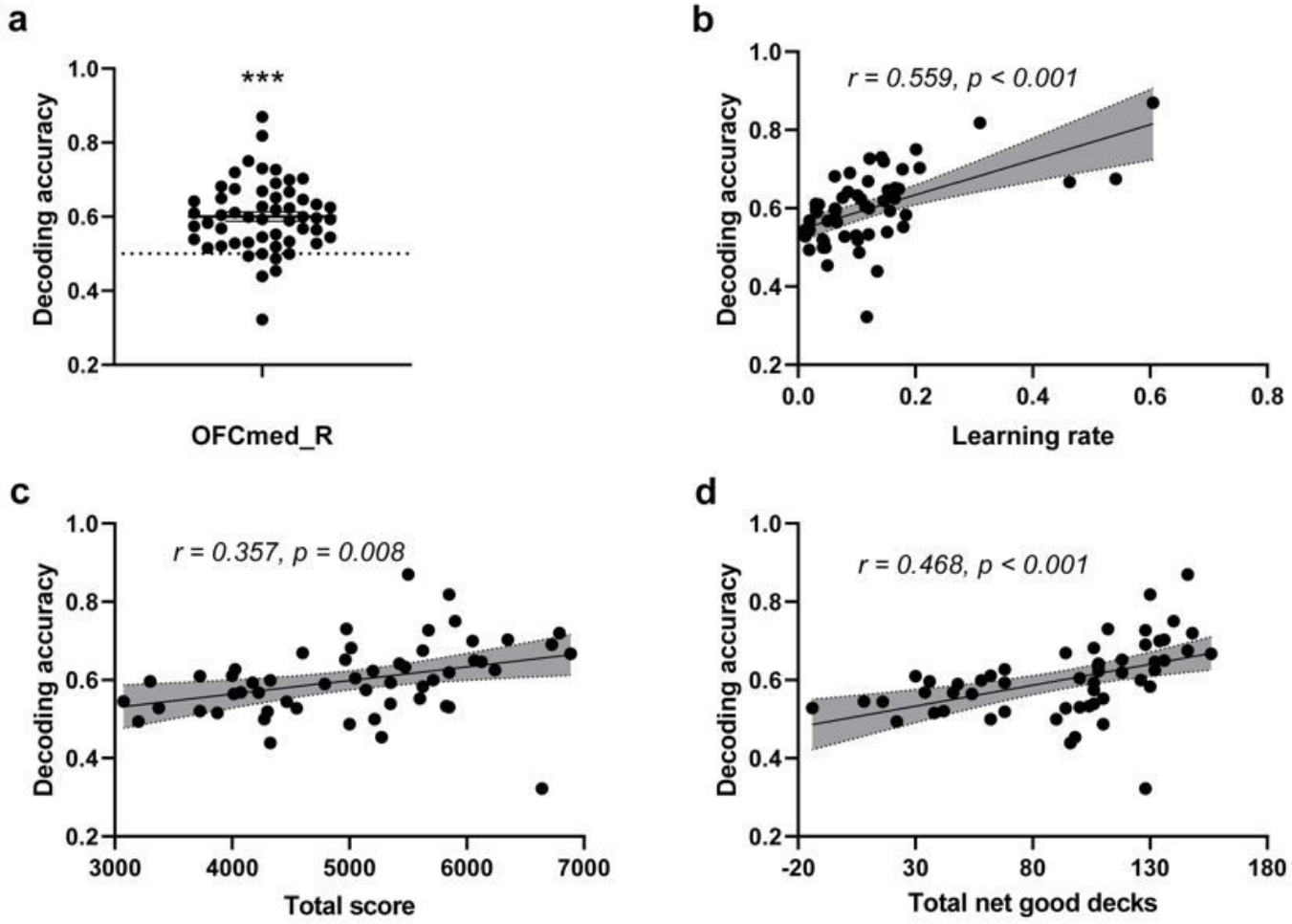

Figure 4

The OFC represents an advantageous choice, and the OFC decoding accuracy is correlated with behavioural performances.

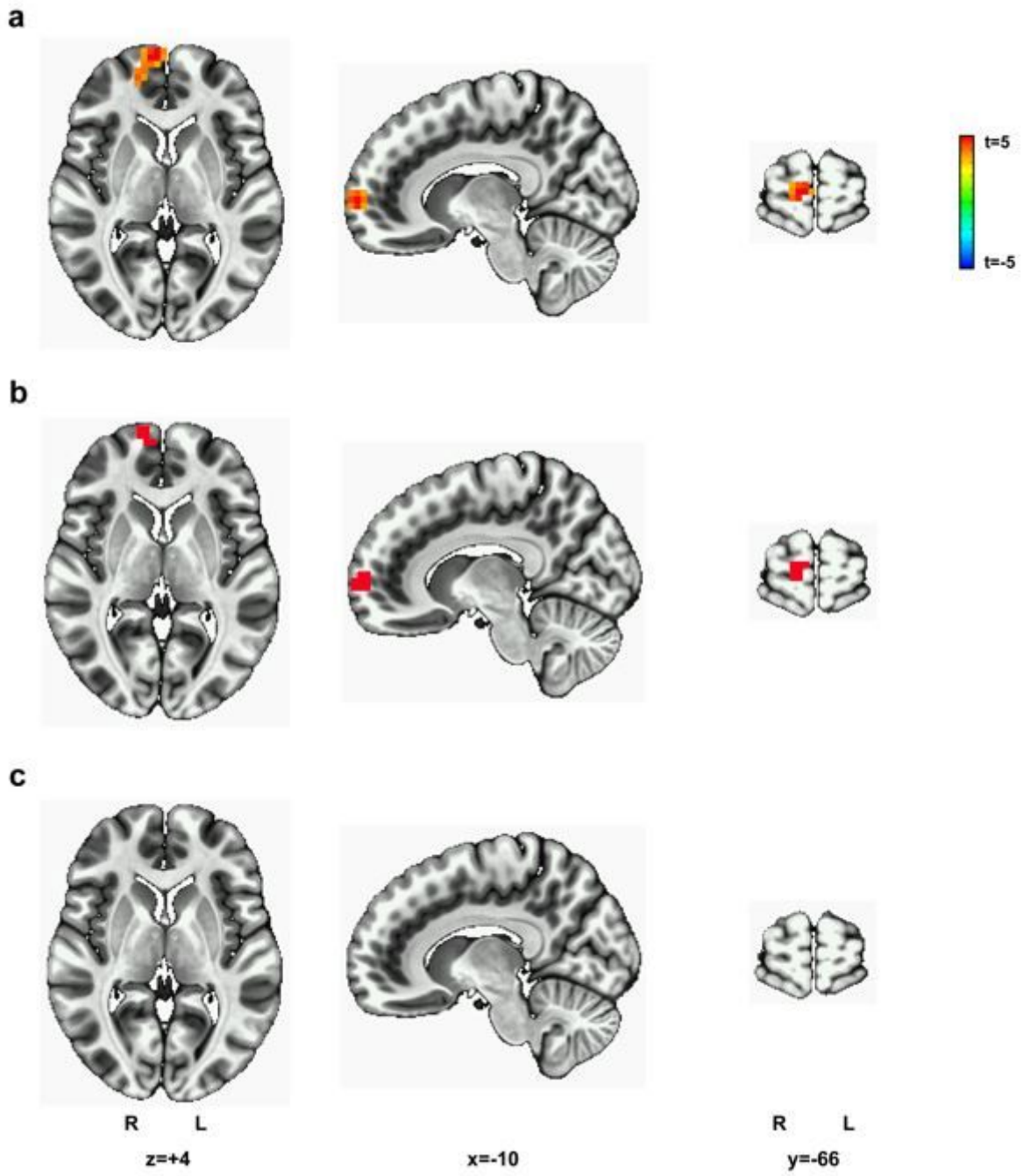

Figure 5

The OFC is functionally connected with the superior medial gyrus for choice, but not for values.

Supplementary Files

This is a list of supplementary files associated with this preprint. Click to download.

- SM.docx